DOI: 10.21062/mft.2024.080 http://www.journalmt.com

Flexible Strain Sensor Based on Metallized Polyurethane Conductive Sponge Using Laser Direct Writing Process

Liang Dong (0000-0003-3441-1468)[1,2], Chen Li (0000-0001-9442-1014)[1,2,3,4*], Peiying Han (0009-0008-5149-1037)[2], Longgang Song (0009-0003-6904-8213)[2], Yangyang Chen (0009-0004-8419-1445)[2]
[1]School of New Energy Engineering & Automobile Industry, Huzhou Vocational & Technical College, Huzhou 313099, China
[2]College of Mechanical & Electrical Engineering, Shaanxi University of Science & Technology. Xi'an, China
[3]School of Mechanical Engineering, Xi'an Jiaotong University, Xi'an 710049, China
[4]State Key Laboratory of Mechanical Manufacturing System Engineering, Xi'an Jiaotong University, Xi'an, China
[*]E-mail: lichen@sust.edu.cn

Flexible strain sensors show great potential in the field of wearables and health monitoring. However, the application of traditional strain sensors on flexible substrates is still limited, and the development of sensors with high sensitivity, excellent stability and good durability is a current research focus. Aiming at the limitation of traditional strain sensor in flexible materials, a flexible strain sensor based on Kirigami structure is proposed. In this study, a Metallized Polyurethane Conductive Sponge (MPCS) was used as the sensor substrate. In the preparation process, we used laser direct writing process to achieve the preparation of highly accurate, patterned sensitive structures. In addition, the length parameter of rectangular hollow structure is optimized by finite element analysis to improve the stability of the sensor. The experimental data show that the prepared flexible strain sensor has a high strain range (130%), a maximum sensitivity of (GF=1.184), a response/recovery time of 168/186 ms, a good linearity, and a very good repeatability and stability during 2000 working cycles. The preparation method provides an effective means for realizing high-performance flexible thin film sensors, and has broad application prospects in intelligent wearable devices, human-computer interaction, health monitoring and other fields.

Keywords: Polyurethane, Porous material, Flexible sensor, Laser direct writing technology, Kirigami structure

1 Introduction

In the field of smart wearable devices and soft robots, flexible strain sensors have attracted much attention because of their high sensitivity, good adaptability and comfort. These sensors can detect and respond to small deformations, providing new solutions for human motion capture, health monitoring and human-machine interfaces [1-3]. Flexible film sensor with its excellent flexibility and ductility, can adapt to complex environment and curved surface, greatly improve the convenience and accuracy of measurement [4, 5]. At its core are the unique properties of flexible substrates and sensitive elements that are flexible, ductile, able to withstand large deformations and maintain electrical properties. Strain sensors based on polyurethane have attracted attention for their flexibility, durability and biocompatibility [6, 7]. Research has focused on improving sensing performance and multifunctional integration, optimizing strain response by manipulating microstructures, introducing micropores or nanofillers, and adding carbon black or metal nanoparticles to enhance electrical conductivity and stability [8-11].

Zhang et al. [12] proposed a novel method for preparing polydimethylsiloxane/graphene nanocomposite conductive materials, and successfully prepared a sandwich type flexible strain sensor. Tests show that the stress and strain of the sensor are linear, and the measurement factor gradually decreases with the increase of the graphene content, and the sensor shows excellent stability. Iqra et al. [13] developed a low-cost flexible piezoresistive strain sensor using reduced graphene oxide and polydimethylsiloxane, which has a flexible structure and a wide sensing range. Hand tests show that the sensor can effectively detect joint movement, demonstrating the ability to monitor muscle movement. Yang et al. [14] prepared a highly sensitive flexible composite pressure sensor with excellent sensitivity, fast response time and cycle stability by using a prestrain strategy. The sensor can detect the human pulse and recognize the roughness of different surfaces, which provides strong support for improving robotic hands and human wearable devices. Feng et al. [15] used salt particle precipitation and mechanical coating methods to fabricate porous graphene nanoplates/polydimethylsiloxane flexible sensors for structural health monitoring. The sensor has the characteristics of high sensitivity and fast response, showing

great potential in the field of structural health monitoring.

Although a lot of efforts have been made in the development of flexible sensors, it is still a big challenge to develop flexible sensors with large range, lightweight, high sensitivity, high stability and long working life [16-19]. Inspired by Kirigami [20-23], a simple process for making flexible thin-film strain sensor is proposed in this the present study. The commercially available MPCS [24, 25] was used as the sensitive element of the sensor. The material was polyurethane sponge as the base material and nickel, copper and other metals were deposited ionic on the base material by electrochemical method. Finally, it is prepared by reduction treatment and has the characteristics of good permeability, electrical conductivity, mechanical stability and low modulus. Thanks to the primary deformation of the Kirigami structure and the secondary deformation of the porous structure of the material itself, the sensor exhibits a large strain range (maximum tensile 130%). Due to the secondary deformation of the Kirigami structure and the porous material, the sensor exhibits a large strain range, the maximal measurement coefficient is 1.184, the response/recovery time is short (168/186 ms), the tension limit can be detected, the repeatability is good, more than 2000 working cycles.

2 Experimental

2.1 MPCS Sensor design

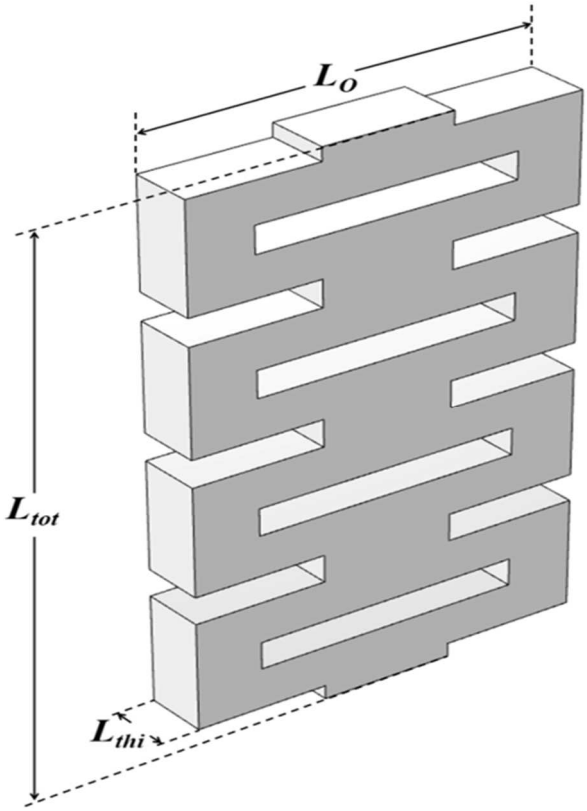

Fig. 1 *Rectangular hollow pattern inspired by Kirigami*

Flexible film sensor with its unique flexibility and ductility, can adapt to a variety of complex environments and surfaces, thus greatly improving the measurement convenience. Inspired by Kirigami structure, this paper presents a flexible thin-film sensor with simple technology. Its pattern is shown in Fig. 1. The Kirigami structure is characterized by the ability to achieve complex deformation through fine cutting and folding while maintaining the stability of the overall shape. This characteristic makes the Kirigami structure can be used as a sensitive element in the flexible stress-strain sensor, and the structural deformation is caused by the change of external stress, which is converted into an electrical signal output. The sensor makes use of the deformation sensitivity and good flexibility of the Kirigami structure to achieve accurate measurement of small stresses and strains. The sensor adopts an axisymmetrically distributed rectangular hollow pattern with a total length L_{tot} of 20 mm, an outer width L_O of 12 mm, and a thickness L_{thi} of 2 mm.

The sensitive structure is segmented into a unit structure, as shown in Fig. 2. In the stretched state, it can be approximately reduced to a hexagon. In order to simplify the design, fixed the hollow rectangle width W_I of its unit structure to 1 mm. Without considering the ductility of the metallized polyurethane porous material itself, the theoretical maximum tensile strain length L_Y of the Kirigami structure is as:

$$L_Y = L_I - L_J = L_I - (L_O - L_I) = 2L_I - L_O \quad (1)$$

Where:

L_I…The outer width of the unit structure [mm],

L_J…The length of the joint of the unit structure [mm].

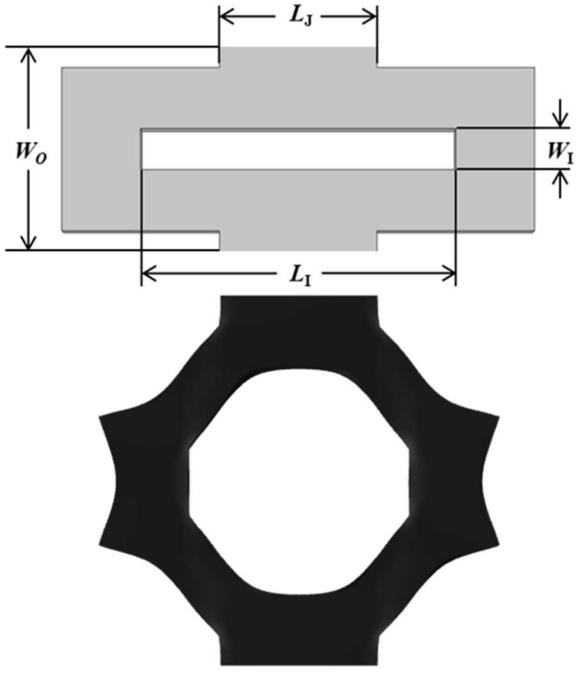

Fig. 2 *Front view of the unit structure of the sensor*

Then the elongation λ of the sensor is as:

$$\lambda = \frac{L_Y}{W_O} = \frac{2L_I - L_O}{W_O} \quad (2)$$

Where:

W_O…The outer width of the cell structure [mm].

2.2 MPCS sensor simulation

The stress and strain of the sensor during tensile process was determined by finite element analysis. For MPCS materials, the Mooney-Rivlin two-parameter hyperelastic model was used to conduct nonlinear static simulation. The material parameters were shown in TAB. 1, and the parameter values were obtained by performing a quasi-static tensile test using the digital push & pull tester.

By finite element simulation, one end of the sensor is fixed and constrained, and the other end is stretched in the z direction, and the displacement is 20%, 40%, 60%, 80% and 100% of the original length of the sensor, respectively. The stress magnitude and distribution under different strain conditions are compared. Set the L_I parameter to 7 mm, 8mm, 9 mm and 10 mm, respectively. Fig. 3 shows the Von Mises stress nebulogram under different tensile states when the length parameter of the hollowed rectangle is 8 mm.

Tab. 1 *Material parameters of MPCS*

Parameters	C_{10}/Pa	C_{01}/Pa
Value	3.60547×10^4	5.52351×10^4

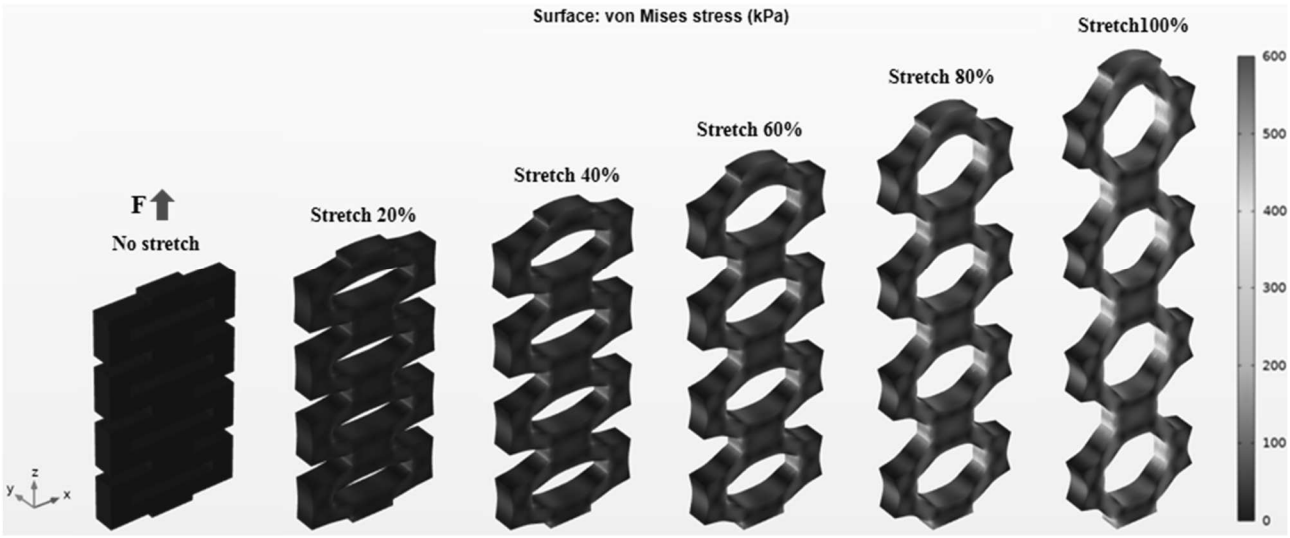

Fig. 3 *Stress nebulae of a sensor with a rectangle length parameter of 8 mm*

Fig. 4 shows the strain and stress relationship of the sensor with different length parameters of the hollow rectangle obtained by the finite element simulation software. As can be seen from the figure, under the same strain degree, the longer the length parameter of the hollow rectangle, the smaller the tension it is subjected to; In other words, for stress measurement, if you want to improve the stress sensitivity of the sensor, you need to increase the length of the hollow rectangle as much as possible. Through comparison, it is found that the stress distribution is generally more uniform when the length parameter of the hollowed rectangle is 8 mm and 9 mm. Only when the hollowed rectangle is under large strain, there are a few stress concentration phenomena inside and outside the edge of the hollowed rectangle. Theoretically, this kind of design has a longer service life. Considering the stress sensitivity, service life and convenient measurement, the length parameter of the hollow rectangle is determined to be 8 mm.

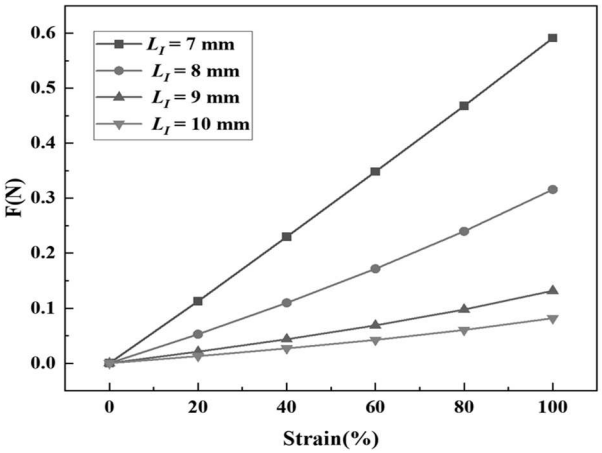

Fig. 4 *Strain and stress relationship of sensors with different rectangle lengths during tensile*

2.3 MPCS sensor fabrication

The main materials and equipment used for sensor fabrication and testing are shown in TAB. 2.

Tab. 2 *Information about the main materials and equipment*

Materials and equipment	Brands and specifications	Manufacturers
Conductive silver paste	2mm	Shenzhen Aodingchang, China
Copper foil tape	K-818	Zhuhai Kingsname, China
Laser marking machine	Mileqi, 0.06mm	Shenzhen Biaozhi, China
Digital push & pull tester	HG-LU-5	Wuhan Huagong, China
Oven	HP-50	Yueqing Handpi, China
Linear displacement platform	101-1SB	Shaoxing Huyue, China
Conductive silver paste	M-4143PD	Physik Instrumente, Germany

The manufacturing process of the sensor is shown in Fig. 5. First, the MPCS film is patterned by laser marking machine, laser direct writing technology can easily obtain the designed structural pattern samples. The sample was then washed with anhydrous ethanol ultrasonic for 20 minutes, and then baked in a drying oven at 150 ℃ for 30 minutes. Conductive silver paste were coated on both sides of the pole and left to dry at room temperature for 5 hours. copper was then affixed to the pole foil, and finally solder the wire to the copper foil strip with an electric iron to lead out the electrode.

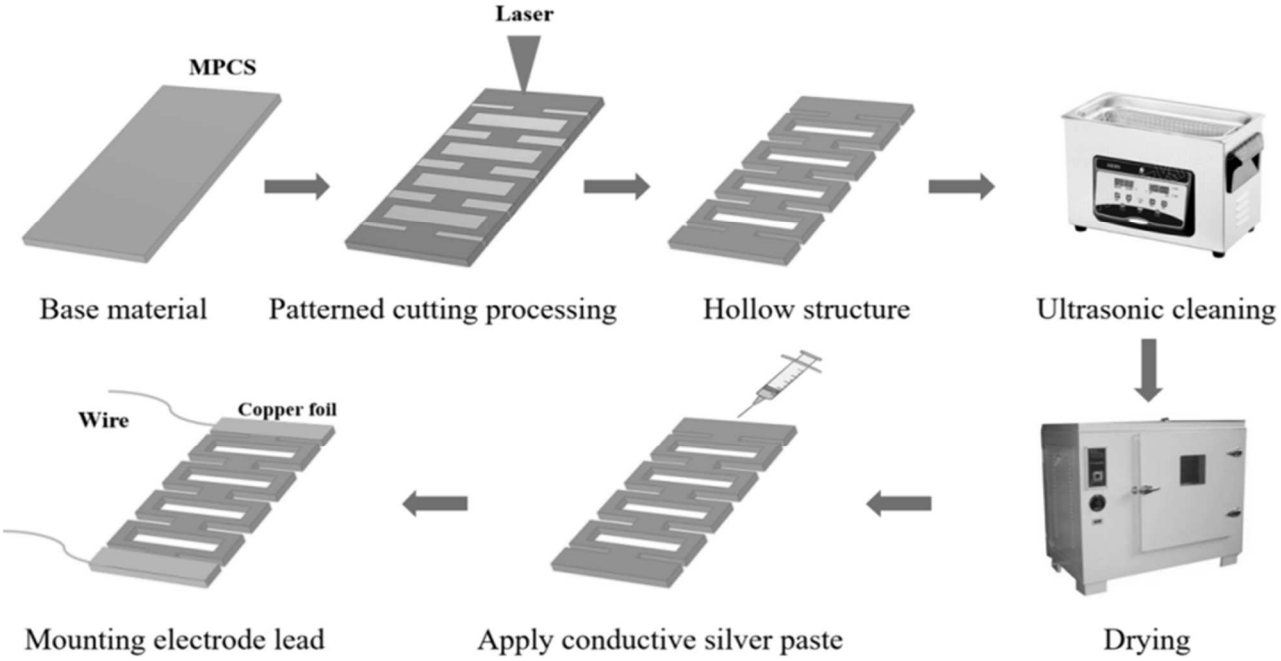

Fig. 5 *Strain and stress relationship of sensors with different rectangle lengths during tensile*

3 Results and discussion

3.1 Characterization

The sensor is installed on the linear displacement platform shown in Fig. 6 to test the working performance of the MPCS strain sensor. Fig. 7~Fig. 9 shows the initial state of the sensor, the state diagram of the sensor when the sensor is stretched by 50%, and the state diagram when the sensor is stretched by 100%, respectively. Observe the size of the displacement and record the change of its resistance value. Repeat the experiment 5 times to take the average value as the data. Interestingly, the sensor is different from the general type of stress-strain sensor, and its resistance variation trend is: with the increase of tensile displacement, the overall resistance decreases in the range. At very low strain (0~8%), the resistance of the sensor increases very briefly during the tensile process, which is due to the existence of micro-cracks in the conductive skeleton of the sensor; When the strain exceeds 8%, the resistance value of the sensor begins to decline rapidly, until the tensile value is about 30%, the decline trend begins to slow down, and the maximum tensile value is close to 95%, which is due to the shrinkage phenomenon of the conductive skeleton due to the Poisson effect during the tensile process, and the skeleton produces different degrees of conductive contact, thus making the resistance decline. When the strain exceeds 95%, the resistance value of the sensor starts to remain basically unchanged and then increases very slowly. After continuing to stretch more than 110%, the resistance value begins to increase rapidly. At this

time, the conductive skeleton micro-crack has obvious expansion phenomenon, which occupies a dominant position. The results of many tests show that the maximum strain ratio of the sensor is about 130%, and the monotonic decline range of the resistance value is about 8% ~95%.

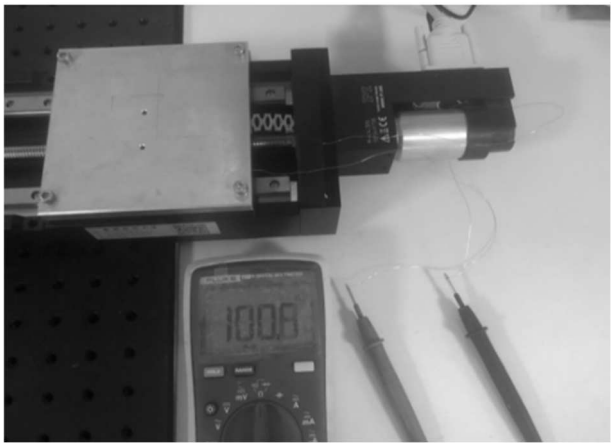

Fig. 6 *Sensor tensile performance measurement device*

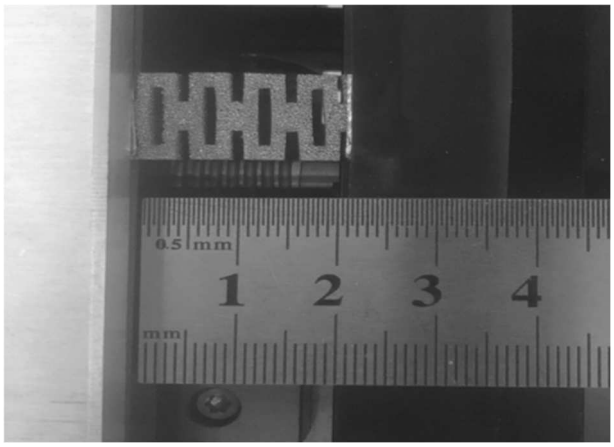

Fig. 7 *Initial state of the sensor*

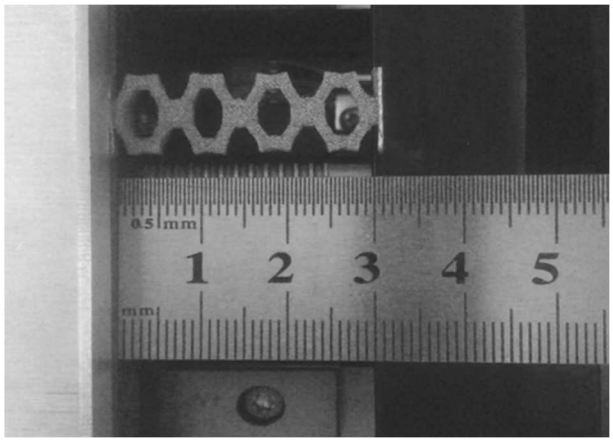

Fig. 8 *Sensor strain 50%*

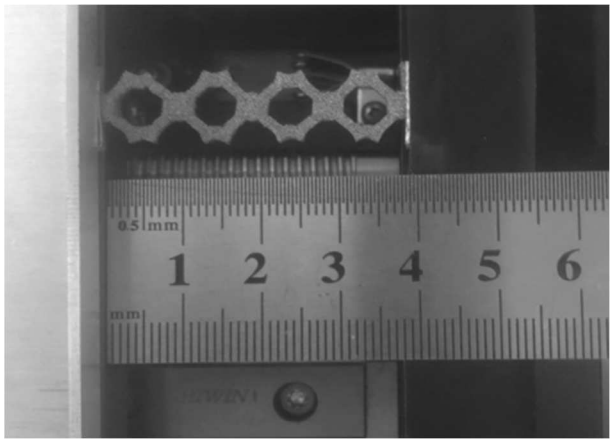

Fig. 9 *Sensor strain 100%*

3.2 Measurement of MPCS sensor

Fig. 10 shows the relationship between the resistance change rate of the sensor and the tensile strain. The sensitivity of the sensor is quantitatively expressed by calculating the ratio of resistance change rate to strain, which is calculated by:

$$GF = \frac{\Delta R / R_0}{\varepsilon} = \frac{(R - R_0)/R_0}{\Delta L / L_0} = \frac{(R - R_0)/R_0}{(L - L_0)/L_0} \tag{3}$$

Where:

$\triangle$R…The amount of change in resistance of the sensor [Ω],

R_0…The initial resistance value of the sensor [Ω],

R…The immediate resistance value of the sensor after the strain [Ω],

$\triangle$L…The amount of change in the length of the sensor [mm],

L_0…The initial length of the sensor [mm],

L…The immediate length of the sensor after the strain [mm].

As can be seen from the figure, in the medium-low strain part of the sensor (8%~30%), GF is 1.184, and R^2 is 0.963; while in the high-strain part (30%~95%), the sensitivity is decreased, GF is 0.24, but the coefficient of determination is still maintained at a high level of R^2 is 0.966. This series of data shows the performance of the sensor under different strain degrees, indicating that the sensor presents a good linear output on the whole.

Fig. 11 shows the output waveform of the sensor in multiple working periods under different tensile strain degrees and shows the resistance change rate curve of the sensor output when the sensor is stretched from 10% to 80%. During the working period, the output consistency is good, the waveform repeatability of multiple periods is good, and the sensor shows good working stability.

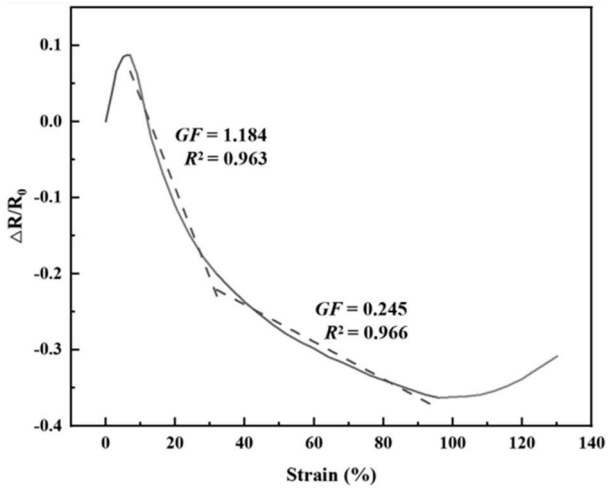

Fig. 10 *The relative resistance change rate of the sensor - strain relationship*

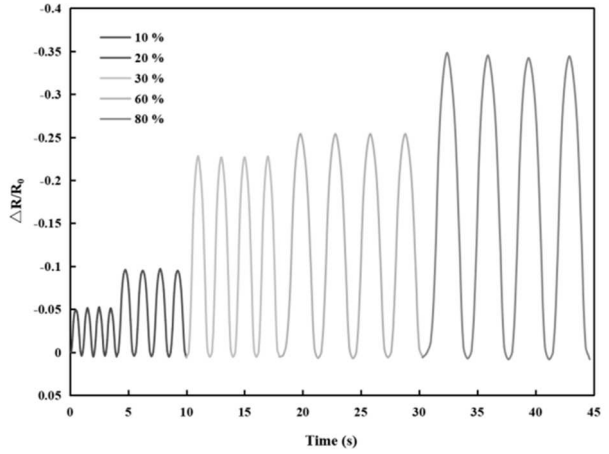

Fig. 11 *The relative resistance change rate of the sensor under periodic load - time relationship*

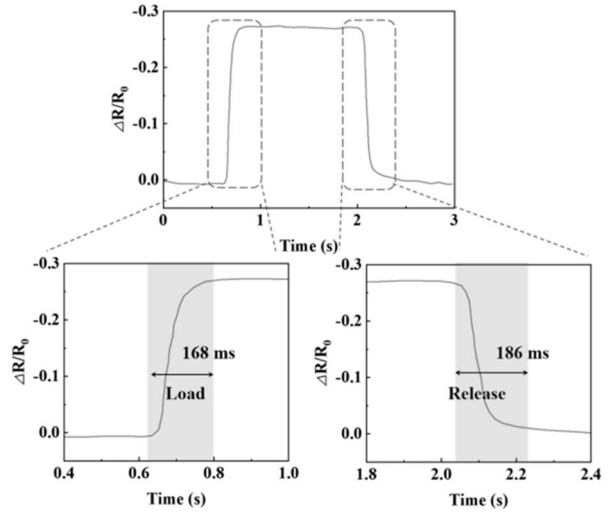

Fig. 12 *The response/recovery time of the sensor*

As shown in Fig. 12, the response time of the sensor is about 168 ms and the recovery time is about 186 ms under the condition of 50% tensile strain degree and 60 mm/s loading/release speed. When the load is withdrawn, the resistance value of the sensor can be quickly restored to the initial value.

Fig. 13 shows the output waveform of the sensor under 50% tensile strain for 2000 working cycles. It can be seen that during the working period, the output amplitude of the sensor remains stable, and the waveform repeatability of multiple cycles is good, and the sensor shows good working stability. The waveforms of the resistance relative change rate of the 991~1000 and 1991~2000 test cycles were intercepted during the test process. Through careful analysis of the waveform data of these specific cycles, it can be found that the range of the resistance relative change amplitude decreased slightly in the later test cycles. After further analysis, it is believed that this change may be due to the fatigue of the sensor in the process of repeated stretching for a long time, resulting in a slight positive drift of the initial resistance value with the tensile fatigue. This drift means that the resistance value of the sensor gradually increases over time, which affects the stability of its output to a certain extent.

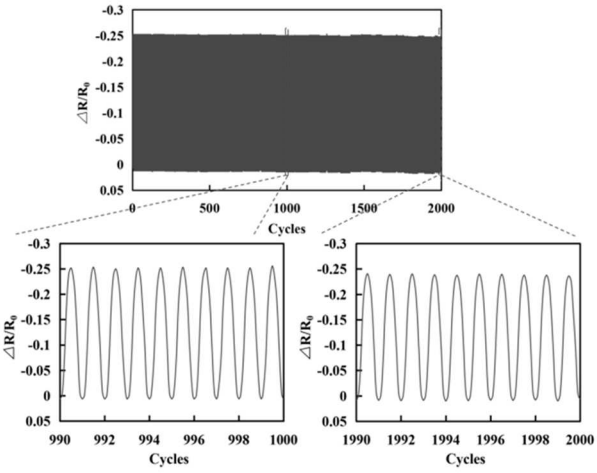

Fig. 13 *The sensor performs 2000 load/release tests at 50% strain*

3.3 Typical application

As shown in Fig. 14, the sensor is mounted on the left index finger of human body, and the two ends are fixed with medical tape, which has a good adaptation effect to the bending deformation of fingers. In order to avoid the rise of resistance in the initial phase of the sensor, a pre-stretch of about 10% is set when fixed. A voltage divider circuit is constructed by connecting sensors in series with a constant resistance, and a constant voltage source is used for power supply. The digital storage oscilloscope is used to record the voltage output of the sensor, and the resistance change rate of the sensor can be further calculated. Fig. 15 shows the response of the sensor to the finger bending Angle. It can be seen that as the degree of finger bending increases, the resistance change rate of the sensor also increases in response.

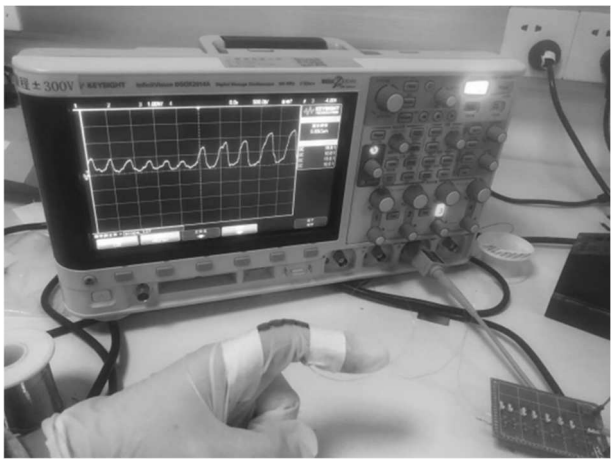

Fig. 14 *The sensor tests the bending Angle of the index finger*

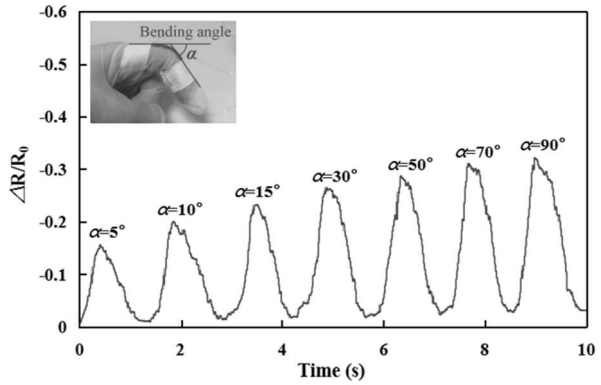

Fig. 15 *The sensor responds to different bending angles of the finger*

4 Conclusions

Inspired by traditional Kirigami structure, an innovative flexible strain sensor design is proposed in this study. Kirigami structure is known for its fine patterns and excellent scalability, which provide a unique perspective for the development of new strain sensors with high sensitivity and excellent scalability. The combination of the Kirigami structure and the porous MPCS material enables the sensor to have extremely low modulus and stiffness, reducing the impact on the measured object, and extending the working range of the sensor with the help of the secondary deformation of the porous structure. The operating range of the sensor is 130%, and the sensitivity is 1.184 (8% ~ 30%), 0.245 (30% ~95%). At a strain degree level of 50% and a speed of 60 mm/s, the response/recovery time of the sensor is about 168/186 ms. The sensor shows excellent cycle stability, and the prepared sensor has certain application value. This study provides a low cost and simple process method for the preparation of flexible strain sensor.

Acknowledgement

This study was fully supported by a grant from the National Natural Science Foundation of China (NO. 52175540) and a grant from China Postdoctoral Science Foundation (NO. 2020M673382) and a grant from the Science and Technology Plan Project of Weiyang District in Xi'an (NO. 202116).

References

[1] HUANG, G., WANG, X., ZHANG, J., WEI, Y., HE, S., WANG, H., & LIU, Z. (2022). Review of MXene nanosheet composites for flexible pressure sensors. *ACS Applied Nano Materials*, 5(10), 14191-14208.

[2] NIE, Z., PENG, K., LIN, L., YANG, J., CHENG, Z., GAN, Q., & Feng, C. (2023). A conductive hydrogel based on nature polymer agar with self-healing ability and stretchability for flexible sensors. *Chemical Engineering Journal*, 454, 139843.

[3] NOVÁK, D., NOVÁK, V., VOŠTINÁR, P., & VOLF, J. (2024). Investigating the pressure distribution on uneven surfaces using an educational robot for development of ergonomic school furniture. *Manufacturing Technology*, 24(1), 98-103.

[4] SURMENEV, R. A., CHERNOZEM, R. V., PARIY, I. O., & SURMENEVA M. A. (2021). A review on piezo-and pyroelectric responses of flexible nano-and micropatterned polymer surfaces for biomedical sensing and energy harvesting applications. *Nano Energy*, 79, 105442.

[5] KARUMUTHIL, S. C., & RAJAN, L. (2023). Optimization of PVDF nanocomposite based flexible piezoelectric tactile sensors: a comparative investigation. *Sensors and Actuators A: Physical*, 353, 114215.

[6] LI, X., KOH, K. H., FARHAN, M., & LAI, K. W. C. (2020). An ultraflexible polyurethane yarn-based wearable strain sensor with a polydimethylsiloxane infiltrated multilayer sheath for smart textiles. *Nanoscale*, 12(6), 4110-4118.

[7] LIU, Z., LI, C., ZHANG, X., ZHOU, B., WEN, S., ZHOU, Y., CHEN, S., JIANG, L., JERRAMS S., & ZHOU, F. (2022). Biodegradable polyurethane fiber-based strain sensor with a broad sensing range and high sensitivity for human motion monitoring. *ACS Sustainable Chemistry & Engineering*, 10(27), 8788-8798.

[8] WANG, P., LI, G., YU, W., MENG, C., & GUO, S. (2022). Flexible pseudocapacitive iontronic tactile sensor based on microsphere-decorated electrode and microporous polymer electrolyte for ultrasensitive pressure detection. *Advanced Electronic Materials*, 8(7), 2101269.

[9] SONG, Y., PENG, C., IQBAL, Z., SIRKAR, K. K., PETERSON, G. W., MAHLE, J. J., & BUCHANAN, J. H. (2022). Graphene oxide and metal–organic framework-based breathable barrier membranes for toxic vapors. *ACS Applied Materials & Interfaces*, 14(27), 31321-31331.

[10] SOUSA, E. A., LIMA, T. H. C., ARLINDO, E. P. S., SANCHES, A. O., SAKAMOTO, W. K., & FUZARI-JUNIOR, G. D. C. (2020). Multicomponent polyurethane–carbon black composite as piezoresistive sensor. *Polymer Bulletin*, 77, 3017-3031.

[11] WANG, Y., CHAO, M., WAN, P., & ZHANG, L. (2020). A wearable breathable pressure sensor from metal-organic framework derived nanocomposites for highly sensitive broad-range healthcare monitoring. *Nano Energy*, 70, 104560.

[12] ZHANG, Z. Q., ZHANG, X. L., XU, G. S., LIU, X. J., GUO, Q., FENG, Z., JIA, J. T., & KU, P. T. (2022). Fabrication of polydimethylsiloxane/graphene flexible strain sensors by using the scraping and coating method. *Review of Scientific Instruments*. 93(6), 5001.

[13] IQRA, M., ANWAR, F., JAN, R., & MOHAMMAD, M. A. (2022). A flexible piezoresistive strain sensor based on laser scribed graphene oxide on polydimethylsiloxane. *Scientific reports*, 12(1), 4882.

[14] YANG, H., SHANG, J. C., WANG, W. F., YANG, Y. F., YUAN, Y. N., LEI, H. S., & FANG, D. N. (2022). Polyurethane sponges-based ultrasensitive pressure sensor via bioinspired microstructure generated by pre-strain strategy. *Composites Science and Technology*, 221, 109308.

[15] FENG, Y., CAI, R., ZHOU, Y., HU, Z., WANG, Y., LIU, D., HAN, S., ZHAO, J., XU, L., & MENG, Q. (2022). A high-performance porous flexible composite film sensor for tension monitoring. *RSC advances*, 12(40), 26285-26296.

[16] NASIRI, S., & KHOSRAVANI, M. R. (2020). Progress and challenges in fabrication of wearable sensors for health monitoring. *Sensors and Actuators A: Physical*, 312, 112105.

[17] YIN, R., WANG, D., ZHAO, S., LOU, Z., & SHEN, G. (2021). Wearable sensors-enabled human–machine interaction systems: from design to application. *Advanced Functional Materials*, 31(11), 2008936.

[18] LI, G., WANG, Y., HUANG, L., & SUN, W. (2022). Research progress of high-sensitivity perovskite photodetectors: A review of photodetectors: Noise, structure, and materials. *ACS Applied Electronic Materials*, 4(4), 1485-1505.

[19] ZHU, W., WANG, J., SUN, W., ZHOU, S., & HE, M. (2023). Preparation of gradient hydrogel for pressure sensing by combining freezing and directional diffusion processes. *Chemical Engineering Journal*, 451, 138335.

[20] SHU, J., WANG, J., LAU, S. C. Y., SU, Y., HEUNG, K. H. L., SHI, X., LI, Z., & TONG, R. K. Y. (2022). Soft Robots' Dynamic posture perception using Kirigami-inspired flexible sensors with porous structures and long short-term memory (LSTM) Neural Networks. *Sensors*, 22(20), 7705.

[21] LI, X., ZHU, P., ZHANG, S., WANG, X., LUO, X., LENG, Z., ZHOU, H., PAN, Z., & MAO, Y. (2022). A self-supporting, conductor-exposing, stretchable, ultrathin, and recyclable kirigami-structured liquid metal paper for multifunctional E-skin. *ACS nano*, 16(4), 5909-5919.

[22] TAO, J., KHOSRAVI, H., DESHPANDE, V., & LI, S. (2023). Engineering by cuts: How Kirigami principle enables unique mechanical properties and functionalities. *Advanced Science*, 10(1), 2204733.

[23] LOW, J. H., CHEE, P. S., LIM, E. H., & GANESAN, V. (2024). Kirigami-inspired self-powered pressure sensor based on shape fixation treatment in IPMC material. *Smart Materials and Structures*, 33(2), 025029.

[24] ZHANG, Y., LIN, Z., HUANG, X., YOU, X., YE, J., & WU, H. (2019). Highly sensitive capacitive pressure sensor with elastic metallized sponge. *Smart Materials and Structures*, 28(10), 105023.

[25] YAN, X., HU, M., LIU, J., YAN, L., ZHANG, N., GAO, J., LIU, J., SHAN, G., & YANG, J. (2020). Compressible metalized soft magnetic sponges with tailorable electrical and magnetic properties. *ChemNanoMat*, 6(2), 316-325.